

EXPERIMENTAL STUDY OF TURBULENT, 2-D, VERTICAL JETS IN SHALLOW WATER

by

P. Espa and A. Frattini

University of Pavia
Department of Hydraulic and Environmental Engineering
Via Ferrata, 1. 27100 – Pavia – ITALY
E-mail paolo.espa@unipv.it

ABSTRACT

This paper reports on an experimental investigation concerning submerged, 2-D turbulent jets in shallow water, impinging vertically onto the free water surface.

Increasing the inlet jet velocity W_0 , a blowing-up develops on the water surface; as W_0 reaches a critical value (W_{0c}), the jet starts to flap and the blowing-up oscillates horizontally, with a characteristic frequency (f_0). Surface oscillations propagate away from the jet in the form of surface water waves (fig. 1).

The hydro-dynamics of this complex flow has so far received little attention in the specialized literature and is still poorly understood. Previous experimental work has mainly focussed on the empirical relations linking the critical velocity W_{0c} and the flapping frequency f_0 to the main flow control parameters (the water depth H and the jet orifice width D).

The present study attempts to cover, at least partly, some lacks of the available material; collected data and observations aim also to help in the validation of numerical models employable for such severe flow simulations.

Differently from the already available experimental works concerning this topic, no wave absorbers at the far ends of the experimental model have been used in order to eliminate wave reflection and to prevent the formation of sloshing standing waves; furthermore, limited water depths H , preventing the studied jets to become fully developed, have been chosen.

For different inlet jet velocities, dye flow visualizations, detailed *LDA* velocity measures and Fourier analysis of the acquired signals have been performed to describe the whole studied flow fields.

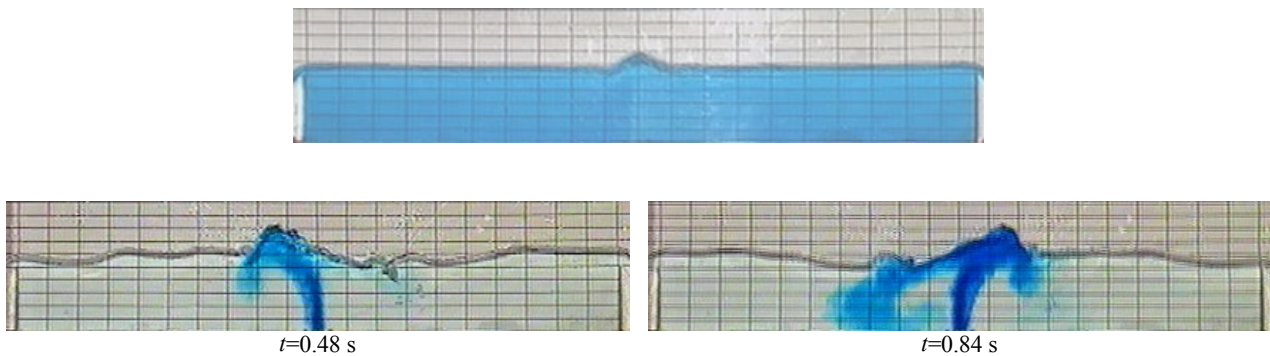


Figure 1. Examples of flow visualizations for growing inlet velocity of the jet:

- stable water surface configuration with blowing-up on the jet axis (up);
- waves generated on the free surface by the jet flapping (down).

1. INTRODUCTION

The study of 2-D turbulent vertical jets injected from the bottom of limited depth water tanks finds important applications in environmental and hydraulic engineering to the analysis of wastewater discharge from linear sources into shallow water bodies. In these cases the upper flow confinement strongly affects its development. The importance of discharges of this kind on the local hydro-dynamics of the interested water bodies is underlined by Jirka (1982).

The turbulent 2-D jet in unconfined environment (*free jet*) is characterized by a *zone of flow establishment (ZFE)* followed by a *zone of established flow (ZEF)*. If Z indicates the distance from the jet orifice and D the orifice length (*jet diameter*), in the *ZFE* the flow structure is affected by the orifice geometry and the region close to the inlet ($Z/D < 6$) is characterized by irrotational flow (*potential core*). In the *ZEF* (see Rajaratnam, 1976) the flow is *self-similar*: the jet spreads linearly with Z and the average velocity along the jet axis decreases as $Z^{-1/2}$. It has been shown (Bradbury, 1965; Gutmark & Wignanski, 1976; Kotsovinos & List, 1982) that the flow becomes well developed for $Z/D \approx 30$.

For upper confined jets, the current impact with the surface delimitating the motion field (this surface may be both a rigid wall and the ambient free surface) generates two horizontal flows moving in opposite directions. Consequently, two further regions are identified: the *zone of surface impingement (ZSI)* and two opposite horizontal flows having the structure of wall jets (*zone of horizontal jets - ZHJ*).

The studies of Jirka & Harleman (1979), Andreopoulos et al. (1986), Kuang et al. (2001) concern turbulent jets vertically impinging the free surface of the ambient fluid. In all these works, the longitudinal extent L of the experimental models is at least twenty times larger than the liquid depth H , thus limiting the influence of the lateral confinement and making reasonable the approximation of infinitely long domains.

Both Jirka & Harleman, (1979) and Andreopoulos et al. (1986), in the case of non-buoyant jet, highlighted the development of re-circulating cells by the sides of the jet. Because of the shallowness of the ambient, not all the fluid entrained by the jet comes from the undisturbed environment; the horizontal surface jets are in fact partly drawn towards the bottom and re-entrained into the vertical jet (fig. 2). The length of the mentioned re-circulating cell is of order $2-2.5H$. This re-entrainment process, reducing the dilution capacity of the discharge, represents a critical eventuality from an environmental point of view.

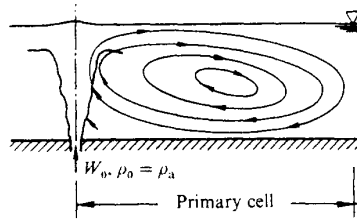


Figure 2. Re-circulating cell activated by a turbulent vertical jet in shallow water (from Andreopoulos et al., 1986).

The experiments conducted by Kuang et al. (2001) led the Authors to accurately state the *ZEF* limits ($30 < Z/D < 100$), where the described jets are self-similar as defined for the free jets.

The quoted works refer however to vertical jets perturbing only very slightly the ambient free surface, which may reasonably be considered horizontal. If W_0 indicates the inlet jet velocity (the ratio between the introduced flow rate Q and the orifice surface A), increasing W_0 a blowing-up of the free surface is determined on the jet axis. Exceeding a critical value of the inlet velocity (W_{0c}), the jet begins to longitudinally oscillate with characteristic frequency f_0 .

The longitudinal oscillation (*flapping*) of turbulent jets in shallow water and more generally the flow characteristics in this conditions have so far received little attention in the specialized literature.

Wu et al. (1998) obtained empirical formulae relating the critical velocity W_{0c} and the frequency of oscillation f_0 with the other control parameters (the water depth H and the jet diameter D). They used a glass paneled box (800 mm long, 1000 mm high and 500 mm thick) equipped with sheets of hogs-hair to dump wave reflection on the lateral walls; since the influence of the lateral walls on the jet oscillations was reduced, the model length was not included among the geometrical parameters controlling the studied flows. Wu et al. (1998) concluded that f_0 is substantially unaffected by W_0 but depends by the liquid depth H following this empirical relation:

$$f_0 = 0.18 \sqrt{\frac{g}{H}}, \quad [1]$$

where g is the gravity acceleration. Furthermore, they found a linear relation between the “critical Froude number” $W_{0c}/(gH_c)^{1/2}$ and the relative liquid depth H/D (applicable only for $H/D > 16$).

$$\left[\frac{W_0}{\sqrt{gH}} \right]_c = 0.018 \frac{H}{D} + 0.357. \quad [2]$$

Another contribution to the analysis of oscillating turbulent jets in shallow water is given by Hsu et al. (2001); the aims and the main conclusions of this study are essentially the same of Wu et al. (1998) but the investigations are conducted with more refined techniques. A much longer experimental model was used (6 m long, 0.4 m high and 0.4 m

thick) but the further control parameters are roughly of the same order of magnitude of those considered by Wu et al. (1998). Furthermore, also in this case, the lateral walls of the experimental model avoided wave reflection phenomena.

The so far produced scientific bibliography concerning turbulent vertical jets interacting with the ambient free surface induces to further deepen this very interesting subject, focussing on conditions where longitudinal oscillations of the jet take place. In particular, laterally confined fluid domains and cases where the limited water depth prevents the jet to become fully developed (i.e. low H/D ratios) are not reported.

2. EXPERIMENTAL SET-UP AND MEASURES OF THE JET FLAPPING FREQUENCY

2.1. Experimental model

The experiments have been conducted in a glass paneled tank, sketched, together with the adopted reference system, in fig. 3. The distance L between the spillways, the spillways height H_s on the bottom of the tank, the thickness S of the tank are fixed respectively to 1000 mm, 98 mm and 30 mm. No devices to avoid wave reflection have been used. On the back side of a transparent panel, a rectangular elements grid has been applied to facilitate geometric observations; the rectangles have 50 mm base and 20 mm height. Ambient temperature water was used.

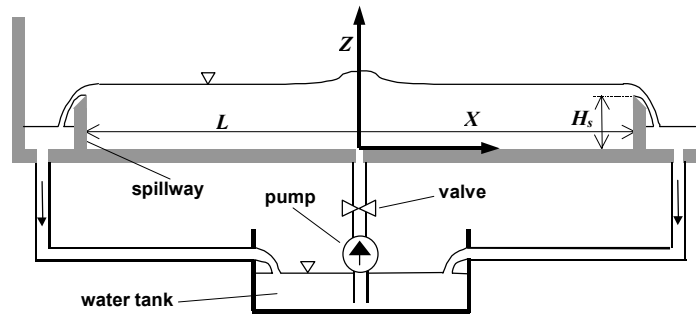


Figure 3. Sketch of the experimental model and adopted reference system.

The model is fed by a pump installed on a water tank whose level is almost constant in the course of the experiments; this tank is fed by the water discharged downstream of the spillways. The flow rate is regulated with a precision valve installed on the discharge side of the pump; the flow rate has been accurately evaluated repeating several measurements of the water volume discharged downstream of the spillways, during long enough time intervals.

The jet is introduced in the tank through an orifice located on its bottom. Two different jet diameters have been considered: $D_1=21$ mm and $D_2=2.6$ mm. In the first case (fig. 4.a), the jet is discharged directly from the internal square section pipe connecting the pump to the model. In the second one (fig. 4.b), in the end part of the mentioned pipe, two plastic plugs have been installed; they possess circumference arc connection followed by a short rectilinear stretch. In both cases, the orifice transversal length is 21 mm and is thus shorter than the model thickness ($S=30$ mm).

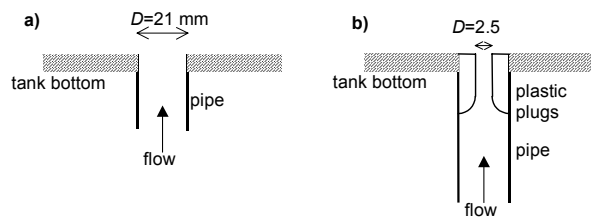


Figure 4. Sketches of the jet orifices in the X-Z plane. a) $D=D_1=21$ mm; b) $D=D_2=2.6$ mm.

2.2. Flow visualizations

In some of the analyzed configurations, images have been collected both to interpret the dynamics of the observed phenomena and to obtain sequences to be compared with the results of numerical simulations of the analyzed flows. The images have been collected with a CCD camera at 25 frames per second sampling rate. The acquired films have first been analyzed with a video-recorder; selected frames have than been digitized and, in some cases, further on processed. In particular, the images have been collected:

- to visualize the free surface motions;
- to visualize the flow in the interior of the model.

In order to obtain a better quality of the visualizations of kind a), colored water has been preferred (using small quantities of methylene blue or ‘‘Congo’’ red). Visualizations of kind b) have been performed introducing in the pipe feeding the model defined volumes of tracer (watered down methylene blue with mass concentration of order 0.5%); the

tracer has been injected in the mentioned pipe with a syringe. The tracer rate is of order 2×10^{-3} l/s, anyhow less than 0.6% of the water flow-rate and so not able to significantly alter the characteristics of the investigated flows.

2.3. LDA velocity measurements

Velocity measurements have been carried out with a single component Laser Doppler probe (*TSI – LDP 100*) working in back scattering mode, with 50 mW power, 694 nm wavelength and equipped with a 250 mm focal length lens. The measures have been executed only in the longitudinal symmetry plane of the tank (*X-Z* plane of fig. 3). The measure volume has approximately the shape of an ellipsoid, with rotation axis orthogonal to the *X-Z* plane and volume of about 0.03 mm^3 . To increase the quality of the signal, the flow has been seeded with titanium dioxide particles, with average diameter of $0.22 \mu\text{m}$ and mass concentration of order 10^{-6} . In some cases, the breaking of the waves on the free water surface drags air bubbles into the flow, determining an error in the *LDA* measures difficult to quantify. Consequently, in some analyzed configurations, it was no possible to execute *LDA* measures in the whole flow field. The collected signal has been processed with an entirely PC controllable processor (*TSI – IFA 600*) equipped with an appropriate software (*TSI – Laservec 1.0*).

The probe movements in horizontal and vertical directions have been executed using a PC controlled traversing system, with 0.03 mm accuracy, while the transversal probe positioning has been executed manually, with a precision guide installed on the described traverse. Thanks to the observed symmetry of the flow field, *LDA* measurements have been carried out just to the right of the jet axis, only in a half of the flow domain. Each velocity measure includes at least 5000 samples.

Elaborating the instantaneous velocity signals, the corresponding fields of time averaged velocity and turbulent kinetic energy (*TKE*) have been obtained. The last one is defined as:

$$TKE \approx \frac{\overline{U'U'} + \overline{W'W'}}{2}; \quad [3]$$

in equation [3], adopting the standard notations,

- *U* e *W* represent the instantaneous values of horizontal and vertical velocity,
- *U'* e *W'* are the differences (fluctuations) between instantaneous values and corresponding time averaged values;
- the upper line indicates time averaging on intervals long enough to stabilize the averaged values.

It comes clear that in equation [3] the velocity fluctuations normal to the *X-Z* plane are neglected; the adopted instrumentation, in fact, doesn't allow for the *LDA* measure of the transversal velocity component. Nevertheless, the relatively small model thickness induces to retain this simplification reasonable, at least for a first approach analysis.

In each measure station, the frequency analysis has been conducted too. For obvious shortness reasons, this analysis is reported only in two points for each analyzed configuration. One point is located near the jet and is named *P₁* (*X=0.015 m, Z=0.07 m*), the other one is not far from the outlet and is named *P₂* (*X=0.40 m, Z=0.07 m*).

2.4. Measurements of the frequency of longitudinal oscillation of the jet

In the cases characterized by longitudinal oscillation of the jet ($W_0 > W_{0c}$), f_0 has been measured simply timing the intervals employed by the free surface upon the jet to describe about 100 complete oscillations.

TABLE 1.A. SYNTHETIC EXPERIMENTS DATA WITH $D=D_j=21$ MM. TESTS MORE DEEPLY EXAMINED IN THE FOLLOWING ARE EVIDENCED.

Code	Q [l/s]	W_0 [m/s]	Re	H [m]	T_0 [s]	f_0 [Hz]
S1	0.085	0.193	4060	0.1066	-	-
S2	0.203	0.459	9650	0.1134	-	-
S3	0.258	0.585	12290	0.1161	-	-
S4	0.273	0.62	13020	0.1168	-	-
O1	0.291	0.66	13860	0.1176	0.59	1.695
O2	0.296	0.672	14110	0.1178	0.59	1.695
O3	0.338	0.767	16100	0.1196	0.61	1.639
O4	0.345	0.782	16420	0.1199	0.616	1.623
O5	0.39	0.885	18580	0.1218	0.71	1.408
O6	0.4	0.908	19070	0.1222	0.71	1.408
O7	0.432	0.981	20590	0.1235	0.71	1.408
O8	0.444	1.008	21160	0.124	0.706	1.416
O9	0.49	1.111	23330	0.1257	0.7	1.429
O10	0.516	1.17	24580	0.1267	0.69	1.449
O11	0.552	1.251	26280	0.128	0.69	1.449
O12	0.571	1.296	27210	0.1287	0.69	1.449
O13	0.571	1.296	27210	0.1287	0.7	1.429
O14	0.586	1.328	27890	0.1292	0.69	1.449
O15	0.616	1.396	29320	0.1303	0.69	1.449

TAB. 1.B. SYNTHETIC EXPERIMENTS DATA WITH $D=D_2=2.6$ MM.

<i>Code</i>	Q [l/s]	W_0 [m/s]	Re	H [m]	T_0 [s]	f_0 [Hz]
S5	0.094	1.714	4460	0.1072	-	-
O16	0.12	2.203	5730	0.1089	0.53	1.886
O17	0.146	2.675	6950	0.1104	0.558	1.793
O18	0.174	3.189	8290	0.1119	0.563	1.776
O19	0.184	3.368	8760	0.1124	0.565	1.771
O20	0.189	3.46	9000	0.1127	0.563	1.778
O21	0.202	3.696	9610	0.1133	0.569	1.757
O22	0.213	3.893	10120	0.1139	0.575	1.739

Tab. 1 collects the synthetic data of each investigated configuration, subdividing the experiments with $D=D_1$ (tab. 1.a) and the ones with $D=D_2$ (tab. 1.b). Each experiment is marked with a code (first left column) composed by a monogram (S for stationary and O for oscillating) followed by a number. The further columns report respectively: the flow rate introduced in the tank; the average velocity of the jet W_0 ; the Reynolds number $Re=W_0D/\nu$ (where ν is the water kinematic viscosity, assumed constant and equal to 1×10^{-6} m²/s); the mean water depth on the tank bottom H ; the period of the jet longitudinal oscillations T_0 ; the frequency of the mentioned oscillations f_0 .

H has been calculated summing the spillways height H_s to the head over the spillway weir (H^*) necessary to discharge half of the introduced flow rate; H^* has been calculated with the classical Bazin formula:

$$\frac{Q}{2} = 0.4SH^* \sqrt{2gH^*}, \quad [4]$$

where $S=30$ mm indicate the weir width (equal to the model thickness).

The more detailed analysis have been conducted for $D=D_1$ and for three different Re . The lower investigated Re corresponds to a stable stationary configuration, the others to oscillating patterns.

2.5. Frequency of the jet longitudinal oscillation: comparison with literature formulae

In fig. 5 is reported the frequency f_0 as a function of the inlet jet velocity W_0 , in all the investigated flow conditions (tab. 1). As explained, these f_0 values have been obtained for slightly different H . Nevertheless, for the two considered diameters, the range of H is relatively small. In agreement with Wu et al. (1998), it is possible to observe that, also in the analyzed cases, the influence of W_0 on the jet flapping frequency is not very strong.

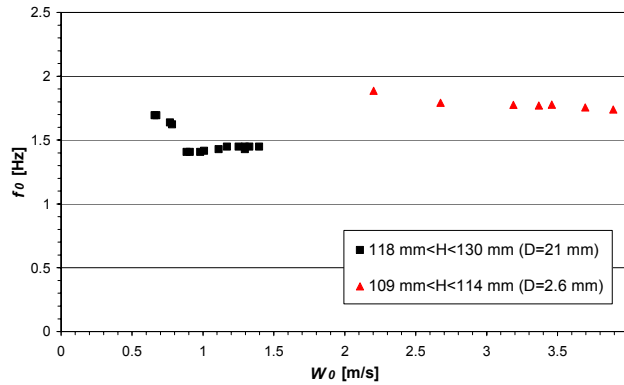


Figure 5. Frequency of longitudinal oscillation of the jet as a function of the average jet velocity in all the conducted experiments.

The diagram of fig. 6 reports f_0 as a function of the liquid depth H , comparing the experimental results with the interpolating relation [1] empirically obtained by Wu et al. (1998). In spite of the mentioned differences between the experimental models employed, the curve of Wu et al. (1998) seems to correctly interpret the observed data, also outside of the validity range of the formula established by the Authors (see case $D=D_1=21$ mm).

Coming finally to the critical velocity W_{0c} , it was chosen to define the last as the upper limit of the velocity range giving stable stationary conditions. To ascertain the stability of a particular configuration, the jet region has been perturbed, generating in the flow longitudinal oscillations with a little rod. If the so forced oscillations quickly disappear and the flow returns stationary, than the configuration is retained stationary. Otherwise, if the oscillations tend to persist, the configuration is declared of transition.

In tab. 2 the so obtained critical velocity values are compared with those calculated with [2] of Wu et al. (1998). The difference between measured and calculated values is certainly not negligible and it is larger for the smaller jet diameter. This discrepancies may be the consequence of two characteristics of the adopted model, both acting to increase the observed W_{0c} (in comparison with the ideal 2-D case) as more as the jet diameter is reduced:

- 1) the orifice width, which is shorter than the model thickness (par. 2.1),
- 2) the small model thickness, which inhibits the development of transversal perturbation; these perturbations may contribute to the start-up of the jet longitudinal oscillations.

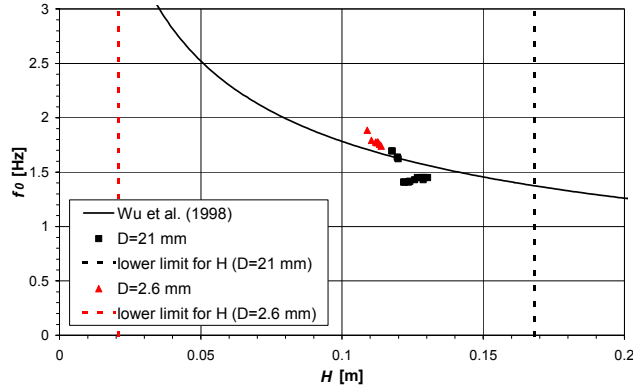


Figure 6. Jet flapping frequency as a function of the mean liquid depth H and comparison with equation [1] of Wu et al. (1998).

TABLE 2. CRITICAL JET VELOCITY: COMPARISON BETWEEN EXPERIMENTAL DATA AND EQUATION [2] OF WU ET AL. (1998).

	$D=D_1$	$D=D_2$
W_{0c} - experimental data	0.62 m/s	1.71 m/s
W_{0c} - Wu et al. (1998)	0.49 m/s	1.13 m/s

3. LIMIT CONDITIONS FOR THE STATIONARY REGIME ($Re=13020$ – EXPERIMENT S4)

The analyzed configuration represents the stability limit of the regime with no longitudinal oscillations of the jet; if W_0 is only slightly higher, the flapping regime becomes stable. The picture of fig. 7 has been obtained averaging ten frames, sampled at regular time intervals of 0.2 s. The average image is obtained transforming first each frame in gray scale, attributing then an integer value to each pixel (value indicating the gray intensity of the pixel) and finally arithmetically averaging the values attributed to corresponding pixels in all the utilized frames. The described operation is useful to cut fortuitous effects as bubbles and spurts, not meaningful to describe the mean motion characteristics. Fig. 7 clearly shows the blowing-up of the free surface on the jet axis, while the remaining part of the free surface maintains itself approximately horizontal, except than near the spillways, where the outlet takes place.

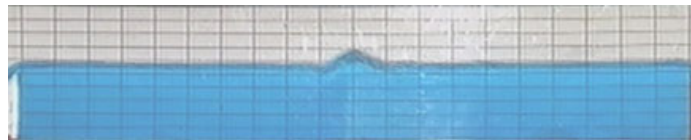


Figure 7. Average image of the free surface obtained with ten equally timed frames.

Fig. 8 reports a sequence of successive frames obtained injecting tracer as described in par. 2.2. By the sides of the jet it is evidenced the formation of two counter-rotating re-circulation cells, also reported for almost horizontal water surface (par. 1). Nevertheless, the major part of the dye tends to flow out the model maintaining itself in the proximity of the free surface (Z_{HJ} – par. 1).

In this configuration, excluding a very small region near the free surface hump, the air dragging doesn't take place. It was so possible to carry out velocity measures on the nodes of a not regular grid, almost covering the entire fluid domain (80 local measurements in all). The time averaged velocity field is represented in fig. 9 and highlights the described re-circulating cell close to the jet. As for the other pictures of this kind, the vectors are drawn normalizing the velocity components to the highest velocity value measured in the considered experiment. The geometric coordinates are both normalized to the spillways height and indicated with small letters ($x=X/H_s$, $z=Z/H_s$).

In fig. 10 is plotted the spatial distribution of turbulent kinetic energy inferred from the LDA measures. As for the other diagrams of this kind, the TKE is normalized to the inlet kinetic energy of the jet ($W_0^2/2$) and the adimensional value is denoted by small letters (tke); also in these diagrams, normalized coordinates are employed. The highest tke values are observed in the region located by the side of the jet and near the free surface, where the jet abruptly expands and slows down (ZSI – par. 1). Another mechanism contributing to increase the tke in this zone may be the strong mixing of the flow coming down from the free surface hump in the ambient fluid below. Near the jet axis, the tke reaches lower values. This fact may be explained by the development, also in the investigated case, of a potential core

region. In the classical case of free turbulent planar jet, the extent of the potential core region along the jet axis is of order $6D$. In the examined conditions ($D=21$ mm, $H=117$ mm), adopting this relation, the mentioned irrotational core should reach the free surface. Of course it doesn't happen, because the upper confinement deflects horizontally the jet. Anyway, by the side of the jet the longitudinal gradients of vertical velocity are not strong enough to determine high tke values. Moving finally in the spillways direction, the vertical gradients of horizontal velocity are also weak and consequently the tke values are low.

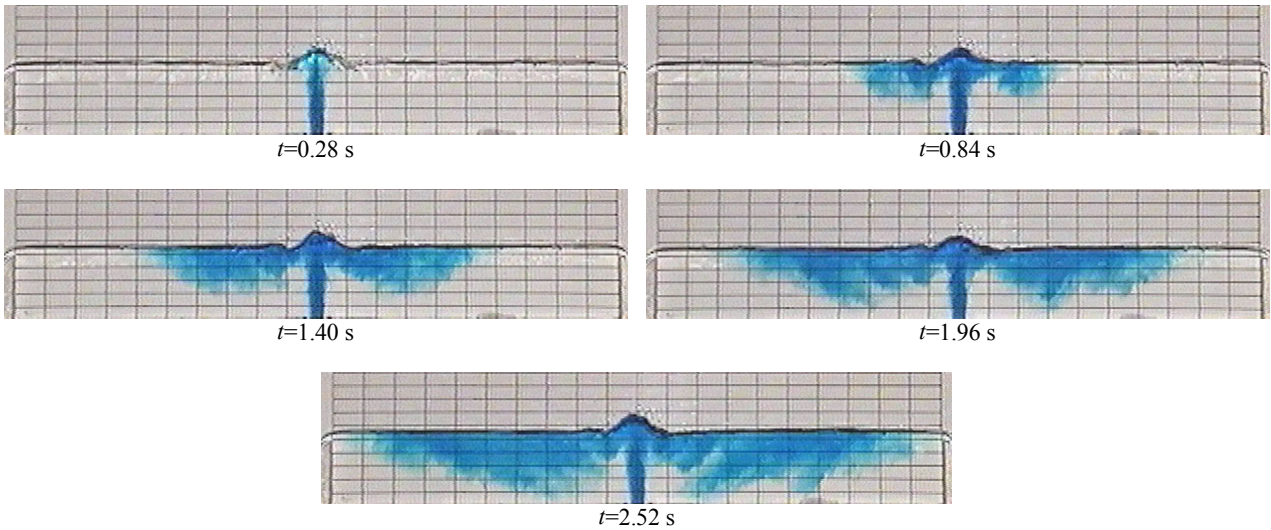


Figure 8. Sequence of images showing the flow pattern for stationary conditions.

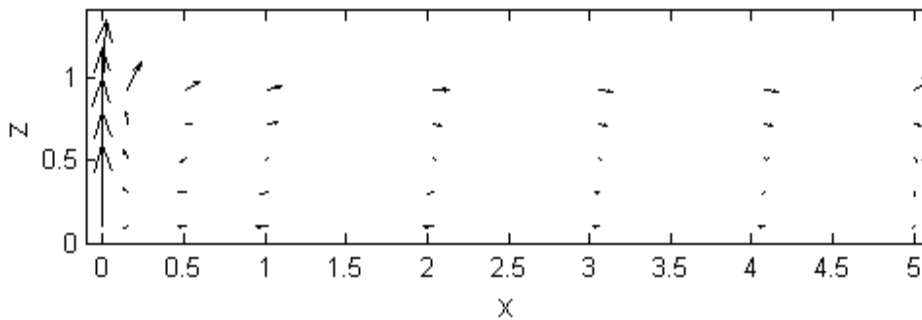


Figure 9. Time averaged velocity field (the maximum velocity has been measured on the jet axis and is equal to 0.75 m/s).

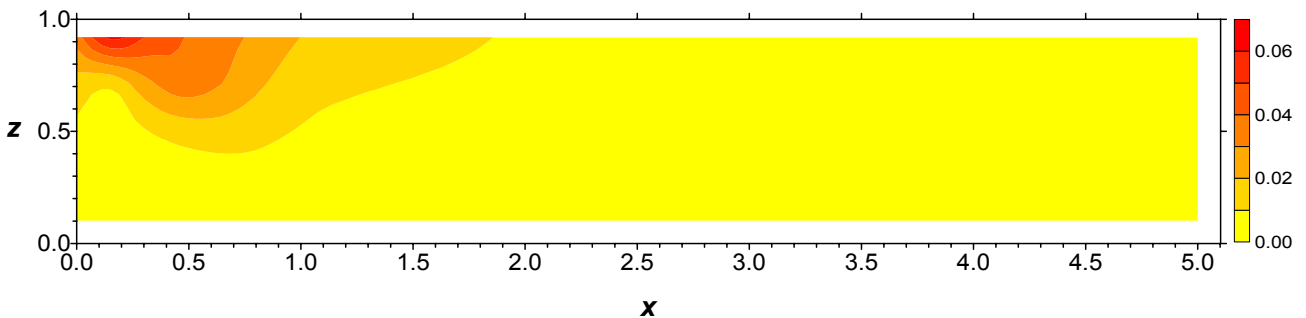


Figure 10. 2-D plot of normalized turbulent kinetic energy for the stationary configuration of experiment S4.

As explained in par. 2.3, the results of the Fourier analysis are reported only in the two points P_1 and P_2 . The diagrams of fig. 11 (but also all the others not reported for shortness reasons) lead to exclude the presence of dominant harmonics modulating the acquired signals, according to the absence of jet flapping and of coherent fluid structures characterized by temporal scales markedly identifiable. As for the other diagrams of this kind, the frequencies are truncated for values whose energy content is of scarce importance. Furthermore, the power spectral density PSD is normalized, as the turbulent kinetic energy, to $W^2/2$ and denoted by small letters (psd).

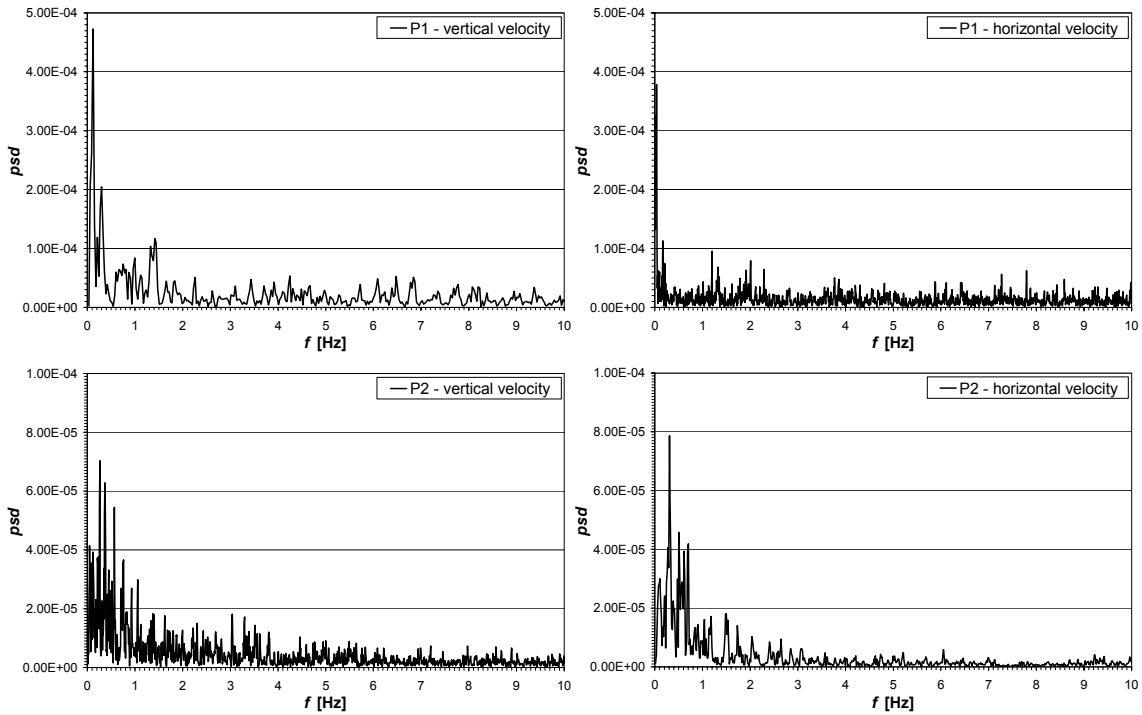


Figure 11. Normalized power spectral density of the vertical and horizontal velocity signal, in points P_1 (up) and P_2 (down).

4. OSCILLATING REGIME ($Re=16420$ - EXPERIMENT O4; $Re=21160$ - EXPERIMENT O8)

The results of two experiments concerning the jet flapping are illustrated; the observed flows show interesting differences and it seemed opportune to highlight them.

4.1. Qualitative analysis of the investigated flows

Fig. 11 reports a sequence of consecutive frames obtained injecting dye in the course of experiment O4, the one with lower Re . The frames have been sampled at time intervals of about a semi-period of the jet longitudinal oscillation.

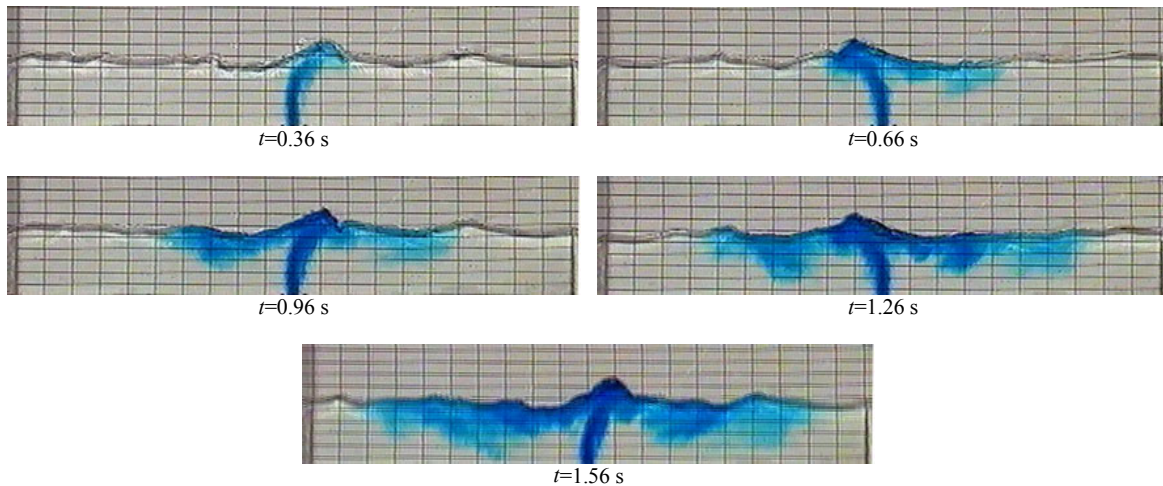


Figure 11. Sequence of frames timed at 0.3 s intervals, for $Re=16420$ (experiment O4).

In spite of the synchronous oscillations of the jet and of the free surface, the tracer diffusion in the motion field follows a pattern similar to that of the analyzed stationary configuration (Fig. 8): the main part of the dye moves towards the outlets remaining close to the free surface and, also in this case, it may be observed the tendency of the tracer to evidence the two counter-rotating re-circulation cells by the sides of the jet, already frequently mentioned.

Fig. 12 reports an analogous sequence concerning the experiment O8. The significant increase of the momentum introduced in the tank, maintaining the fluid depth H almost constant (tab. 1.a), seems to determine a different flow pattern. The fluid flowing down from the hump on the free surface enter violently the ambient fluid, activating two

counter rotating vortices by the sides of the jet. These vortices, differently from the previous cases, are so strong to “trap” (at least during the considered interval) almost the whole injected dye, determining its heap near the jet.

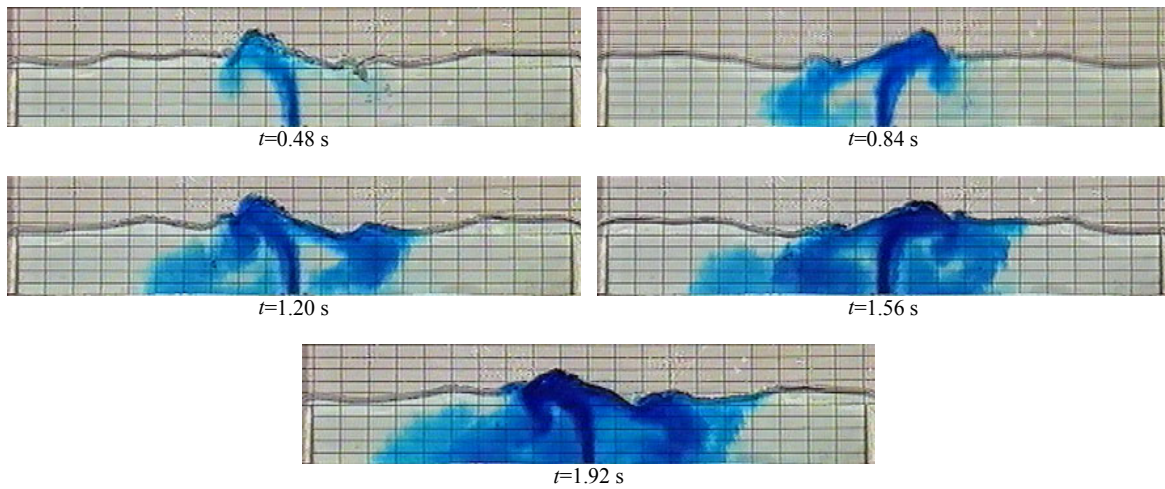


Figure 12. Sequence of frames timed at 0.36 s intervals, for $Re=21160$ (experiment O8).

These visualizations suggest two different flow patterns for the investigated configurations (fig. 13). For the higher Re experiment, the introduced flow rate flows out the model following first the edges of the re-circulations, successively the tank bottom and finally the spillways. These symmetric currents drag two weak vortices close to the free surface, each one rotating in opposite sense than the corresponding one near the jet.

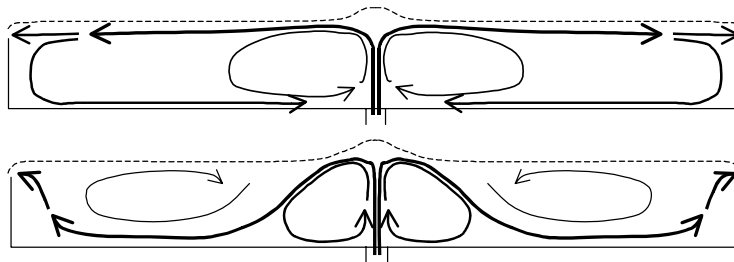


Figure 13. Sketches of the flow patterns of the two analyzed oscillating configurations. a) $Re=16420$; b) $Re=21160$.

In fig. 14 another sequence concerning the experiment O8 is reported. Each image is the average of five homologous frames, i.e. timed by an integer multiple of a complete oscillation period. In spite of the conducted elaboration, in every averaged image the free water surface is very tidy, demonstrating the regularity of the flow oscillations. Since the *LDA* measures in this configurations have not been carried out on the entire flow domain, the images of fig. 14 constitute also a useful tool to compare the results of numerical simulations with experimental data.

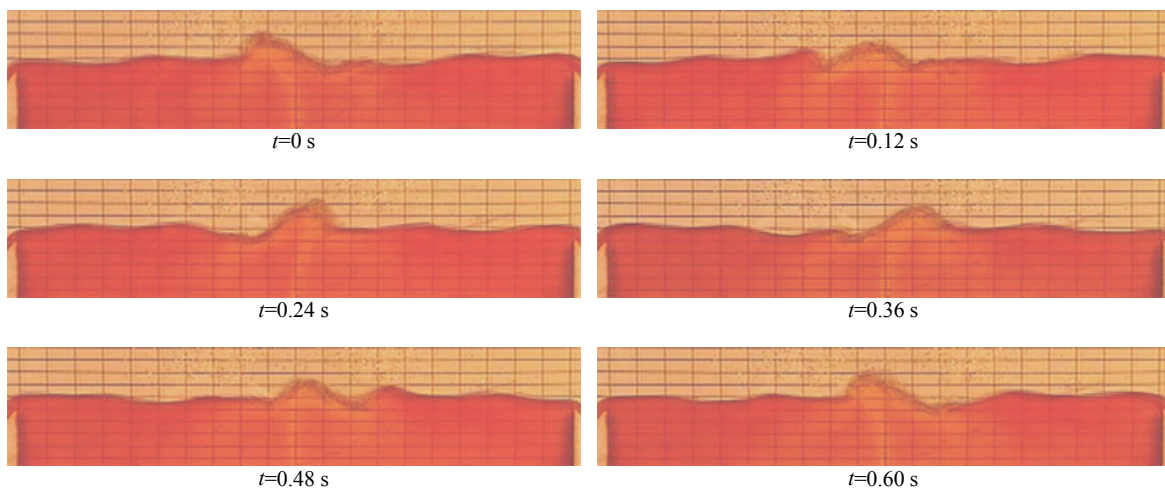


Figure 14. Sequence of averaged images describing a complete period of longitudinal oscillation for $Re=21160$ (experiment O8).

4.2. Quantitative analysis of the investigated flows

In spite of the oscillations of the jet and of the free surface, in experiment O4 the flow doesn't drag air bubbles, thus allowing for *LDA* measures in the whole analyzed domain. Fig. 15 shows the time averaged velocity vector field, inferred from 170 local measurements. According with fig. 11 and fig. 13, the average motion field shows only one clockwise rotating vortex; it also highlights that the free surface horizontal flow directed towards the outlet (*ZHJ* – par. 1), is partly deflected towards the bottom at distance of order $2H$ from the jet axis, thus generating the often mentioned re-circulating cell.

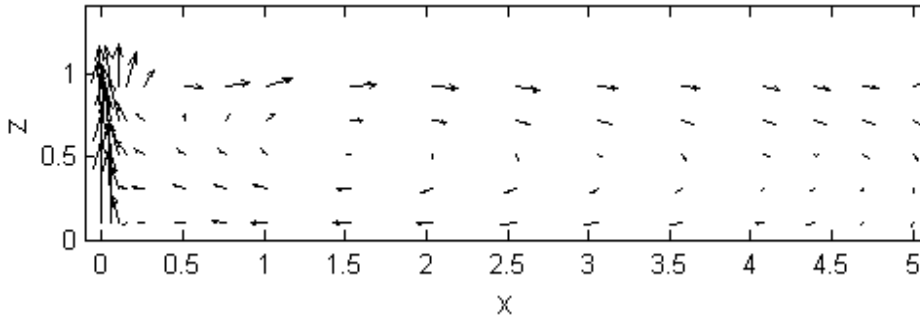


Figure 15. Time averaged velocity vector field for $Re=16420$ (the maximum velocity - 0.95 m/s - has been measured on the jet axis).

In fig. 16 the spatial distribution of normalized turbulent kinetic energy is plotted. It should be noted that in the examined conditions the velocity fluctuations (and thus the *tke* values) include both the high frequency ones (connected to turbulent agitation) and the lower frequency ones (connected to mass oscillations). Close to the free surface and by the side of the jet, the *tke* reaches values three times higher than the stationary case. In the re-circulation region, the measured values are not so high. The mechanism justifying these high *tke* values could be the same described for stationary conditions. It is connected to the jet sudden deceleration near the water surface and to the violent mixing in the ambient fluid of the flow descending the free surface hump generated by the jet. The plot of fig. 16 shows low *tke* levels in an approximately triangular region, bounded by the jet axis and the semi-diameter of the orifice; the shape of this region recalls that of the potential core in the case of planar free jet.

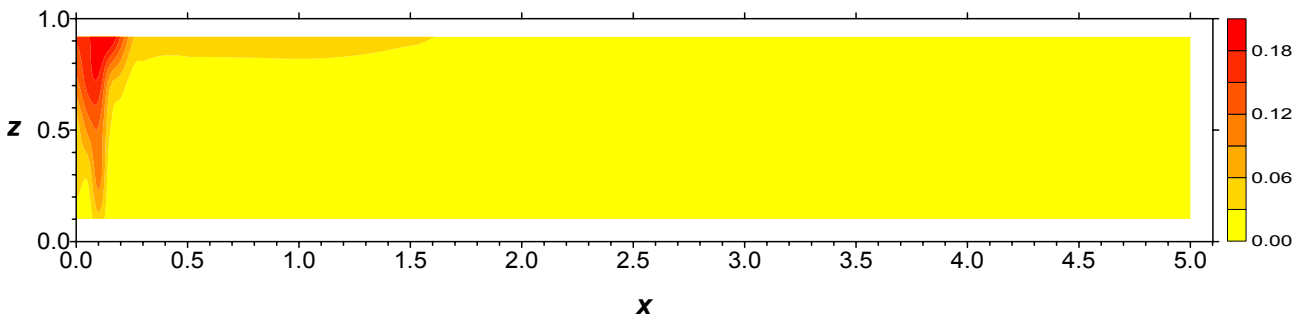
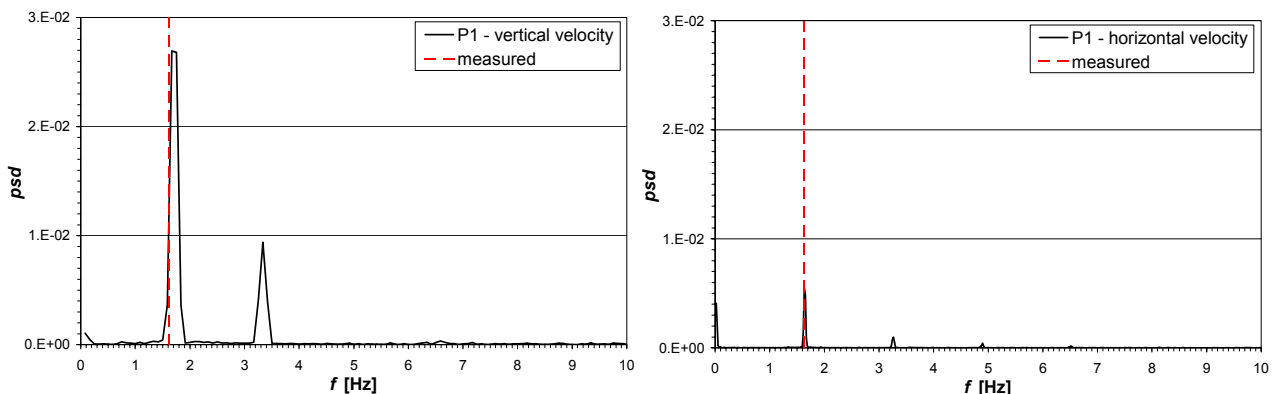


Figure 16. 2-D plot of the normalized turbulent kinetic energy for the oscillating configuration of experiment O4.

The results of the frequency analysis of the velocity signals collected in points P_1 e P_2 are finally reported (fig. 17). The spectra of fig. 17 synthesize some important aspects of the investigated flow.



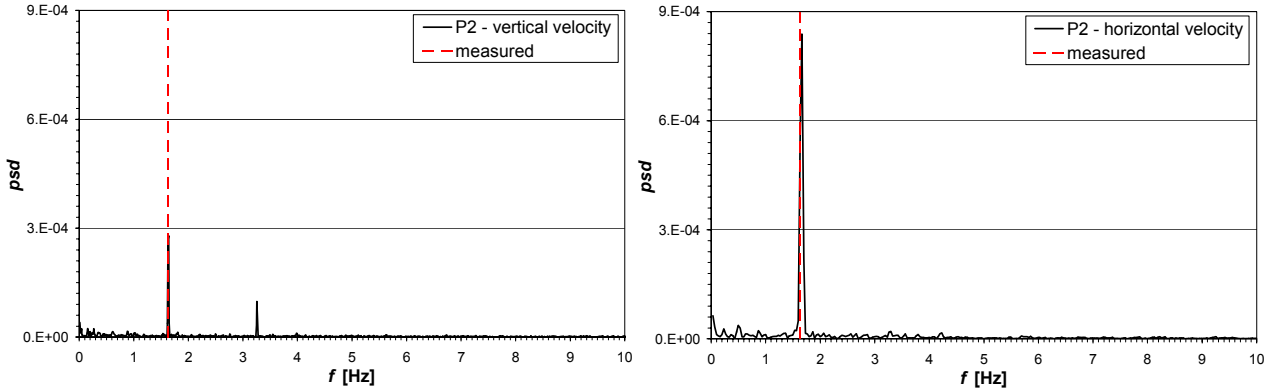


Figure 17. Normalized power spectral density (*psd*) of the vertical and horizontal velocity signals in points P_1 (up) and P_2 (down), under conditions of experiment O4.

The flow is strongly modulated by the jet flapping frequency. The *psd* plots, particularly those concerning the vertical velocity component, show significant energy contents also associated to the second harmonic (the frequency double of the jet flapping one). This phenomenon, probably connected to wave reflection on the vertical spillways delimiting the cavity, has not been observed by Hsu et al. (2001) using a longer model equipped with wave absorbers.

The *psd* peaks of the oscillating case are much stronger than those of the stationary case, being the difference of almost two orders of magnitude for the vertical velocity signal in point P_1 . Furthermore, in the oscillating case, the energy content distributed over the dominant frequencies decreases of about thirty times moving from the jet (point P_1) towards the spillways (point P_2); this reduction is limited to about five times for the stationary case.

Near the jet (point P_1) the *psd* of the vertical velocity is three times larger than the horizontal velocity one, while the contrary takes place near the spillways (point P_2), where the fluid flows towards the outlet, periodically forced by the wave motion generated by the jet flapping, but maintaining prevailing horizontal direction.

For the control parameters of experiment O8 ($W_0=1.01$ m/s, $Re=21160$), the water surface movements cause the dragging of air bubbles in a large portion of the analyzed domain. For this reason, *LDA* measures have been carried out only close to the jet ($0 \text{ mm} \leq X \leq 15 \text{ mm}$) and in the outlet region ($300 \text{ mm} \leq X \leq 490 \text{ mm}$), excluding the vortex zone evidenced in the visualizations of fig. 12. The time averaged velocity vector field (obtained with 90 local measures – fig. 18), in spite of the mentioned limitations, highlights a flow pattern substantially different in comparison with the two already illustrated (fig. 9 and fig. 15). In particular, the time averaged measurements corroborate the flow structure inferred by the flow visualizations and sketched in fig. 13.

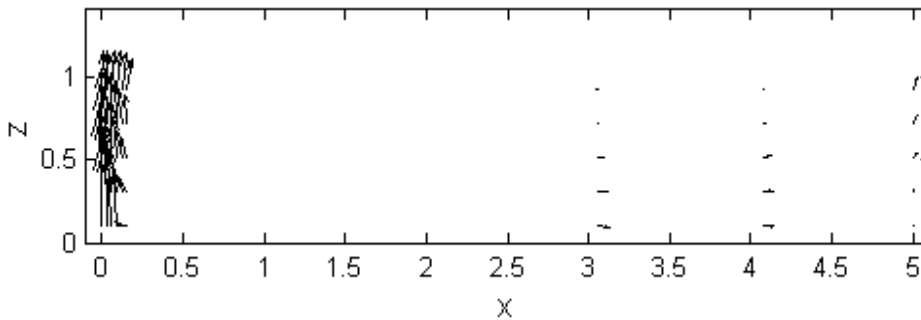


Figure 18. Time averaged velocity vector field for $Re=21160$ (the maximum velocity – 1.23 m/s - has been measured on the jet axis).

Fig. 19 reports the *tke* plot for the maximum analyzed Re . The spatial distribution of *tke* near the jet is, also quantitatively, analogous to the already described one (fig. 16). It is thus possible to extend to this case the precedent considerations. In the outlet region, in spite of the different average flow pattern, the *tke* values are low too, excluding noticeable mechanisms of *tke* transport from the zones where it reaches higher values. Nevertheless, in the not-measured zone it seems reasonable to expect *tke* values higher than those of fig. 16, because of the stronger mixing showed by the flow visualizations of fig. 12.

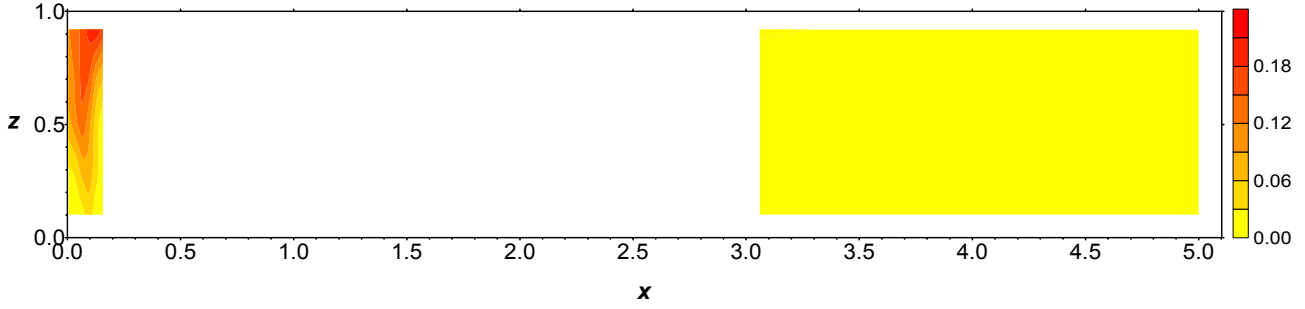


Figure 19. 2-D plot of the normalized turbulent kinetic energy for the oscillating configuration of experiment O8.

The frequency analysis of the velocity signals (fig. 20) leads to considerations analogous to those concerning the already discussed oscillating case. The only difference is the higher energy content of the horizontal velocity signal in the outlet region (point P_2). This increase may be explained considering the dissipation and evacuation of the excess of mechanic energy introduced by the jet in the tank: once the *tkc* production near the jet seems to be saturated, than wider waves develop on the free surface.

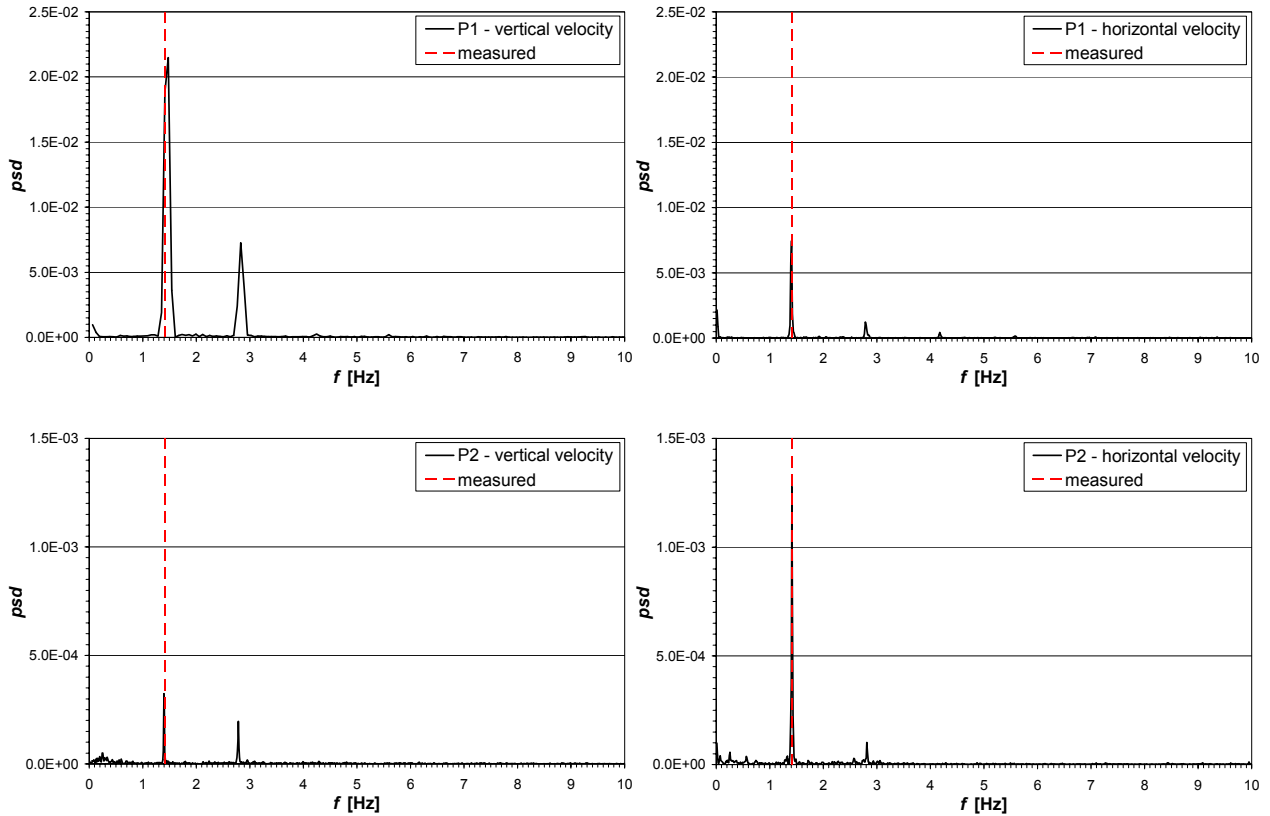


Figure 20. Normalized power spectral density (*psd*) of the vertical and horizontal velocity signals in points P_1 (up) and P_2 (down), under conditions of experiment O8.

5. SUMMARY

A study of turbulent 2-D vertical jets introduced from the bottom of a shallow tank and strongly interacting with the ambient free surface is reported. The employed experimental model is a relatively thin rectangular box, laterally bounded by spillways and not equipped to avoid wave reflection.

For a fixed geometrical configuration, three different Reynolds numbers have been deeply investigated, the smaller one marking the stability limit of non-oscillating pattern and the others concerning jet flapping.

Dye flow visualizations, detailed *LDA* measurements and frequency analysis of the acquired signals are reported for each analyzed *Re*. For the non-flapping configuration and for the low *Re* oscillating one, the average flow pattern is substantially similar and, near the jet, recalls the flow structure described by other Authors in the case of almost horizontal water surface. Noticeable differences between the flow patterns of the two investigated oscillating configurations have instead been observed.

BIBLIOGRAPHY

- Andreopoulos, J., Praturi, A. and Rodi, W. (1986). "Experiments on Vertical Plane Buoyant Jets in Shallow Water", *Journal of Fluid Mechanics*, 168, 305-336.
- Bradbury, L.J.S. (1965). "The Structure of Self-Preserving Turbulent Plane Jet", *Journal of Fluid Mechanics*, 23, pp. 31-64.
- Gutmark, E. and Wygnanski, I. (1976). "The Planar Turbulent Jet", *Journal of Fluid Mechanics*, 73, pp. 465-495.
- Hsu, C.T., Kuang, J. and Sun, J.H. (2001). "Flapping Instability of Vertically Impinging Turbulent Plane Jets in Shallow Water", *Journal of Engineering Mechanics*, 127, pp. 411-420.
- Jirka, G.H. (1982). "Multiport Diffusers for Heat Disposal: a Summary", *Journal of the Hydraulic Division ASCE*, 108, pp. 1425-1468.
- Jirka, G.H. and Harleman, D.R.F. (1979). "Stability and Mixing of a Vertical Plane Buoyant Jet in Confined Depths", *Journal of Fluid Mechanics*, 94, pp. 275-304.
- Kotsovinos, N.E. and List, E.J. (1982). "Plane Turbulent Buoyant Jets. I: Integral Properties", *Journal of Fluid Mechanics*, 81, pp. 25-44.
- Kuang, J., Hsu, C.T. and Qiu, H. (2001). "Experiments on Vertical Turbulent Plane Jets in Water of Finite Depth", *Journal of Engineering Mechanics*, 127, 18-26.
- Rajaratnam, N. (1976). "Turbulent Jets", Elsevier Scientific Publishing Company, Amsterdam, The Netherlands.
- Wu, S., Rajaratnam, N. and Katopodis, C. (1998). "Oscillating Vertical Plane Turbulent Jet in Shallow Water", *Journal of Hydraulic Research*, 36, No. 2, pp. 229-234.